A peer-reviewed version of this preprint was published in PeerJ on 12 April 2017.

Direct imaging of APP proteolysis in living cells

Niccoló Parenti [1,2] , **Ambra Del Grosso** [3] , **Claudia Antoni** [1] , **Marco Cecchini** [3] , **Renato Corradetti** [2] , **Francesco S Pavone** [1,4] , **Martino Calamai** Corresp. [1,4]

[1] European Laboratory for Non-linear Spectroscopy (LENS), University of Florence, Sesto Fiorentino, Florence, Italy

[2] Department of Neuroscience, Psychology, Drug Research and Child Health, University of Florence, Florence, Italy

[3] NEST, Istituto Nanoscienze-CNR and Scuola Normale Superiore, Pisa, Italy

[4] National Institute of Optics, National Research Council of Italy (CNR), Florence, Italy

Corresponding Author: Martino Calamai
Email address: calamai@lens.unifi.it

It is now widely accepted that oligomers consisting of Aβ peptide are the cytotoxic species contributing mostly to the development of Alzheimer's disease. Aβ peptide production results from the specific proteolytic processing of the amyloid precursor protein (APP). Deciphering the factors governing the activity of the secretases responsible for the cleavage of APP is still a critical issue. Kits available commercially measure the enzymatic activity of the secretases from cells lysates, *in vitro*. By contrast, we have developed a prototypal rapid bioassay that provides visible information on the proteolytic processing of APP directly in living cells. APP was fused to a monomeric variant of the green fluorescent protein and a monomeric variant of the red fluorescent protein at the C-terminal and N-terminal, respectively. Changes in the proteolytic processing rate in transfected human neuroblastoma and rat neuronal cells were imaged with confocal microscopy as changes in the red/green fluorescence intensity ratio. The significant decrease in the mean red/green ratio observed in cells over-expressing the β-secretase BACE1 fused to a monomeric blue fluorescent protein confirms that the proteolytic site is still accessible. Specific siRNA was used to evaluate the contribution of endogenous BACE1. Interestingly, we found that the degree of proteolytic processing of APP is not completely homogeneous within the same single cell, and that there is a high degree of variability between cells of the same type. We were also able to follow with a fluorescence spectrometer the changes in the red emission intensity of the extracellular medium when BACE1 was overexpressed. This represents a complementary approach to fluorescence microscopy for rapidly detecting changes in the proteolytic processing of APP in real time. Moreover, we obtained a quantitatively robust estimate of the changes in the red/green ratio for the above conditions by using a flow cytometer able to simultaneously excite and measure the red and green fluorescence. Our novel approach lay the foundation for a bioassay suitable to study the effect of drugs or particular conditions, to investigate in an unbiased way the the

proteolytic processing of APP in single living cells in order, and to elucidate the causes of the variability and the factors driving the processing of APP.

1 **Direct imaging of APP proteolysis in living cells**

2

3 Niccoló Parenti[1,2], Ambra Del Grosso[3], Claudia Antoni[1], Marco Cecchini[3], Renato Corradetti[2],

4 Francesco S. Pavone[1,4] , Martino Calamai*[1,4]

5 [1]European Laboratory for Non-linear Spectroscopy (LENS), University of Florence, Florence,

6 Italy 50019

7 [2]Department of Neuroscience, Psychology, Drug Research and Child Health, University of

8 Florence, Florence, Italy

9 [3]NEST, Istituto Nanoscienze-CNR and Scuola Normale Superiore, Piazza San Silvestro 12,

10 Pisa 56127, Italy.

11 [4]National Institute of Optics, National Research Council of Italy (CNR), Largo Fermi 6, 50125,

12 Florence, Italy

13

14

15 *Corresponding author

16 E-mail: calamai@lens.unifi.it

17

18

19

20

21

22

23

24

25

Abstract

Alzheimer's disease is a multifactorial disorder caused by the interaction of genetic, epigenetic

and environmental factors. The formation of cytotoxic oligomers consisting of Aβ peptide is

widely accepted as being one of the main key events triggering the development of Alzheimer's

disease. Aβ peptide production results from the specific proteolytic processing of the amyloid

precursor protein (APP). Deciphering the factors governing the activity of the secretases

responsible for the cleavage of APP is still a critical issue. Kits available commercially measure

the enzymatic activity of the secretases from cells lysates, *in vitro*. By contrast, we have

developed a prototypal rapid bioassay that provides visible information on the proteolytic

processing of APP directly in living cells. APP was fused to a monomeric variant of the green

fluorescent protein and a monomeric variant of the red fluorescent protein at the C-terminal and

N-terminal (mChAPPmGFP), respectively. Changes in the proteolytic processing rate in

transfected human neuroblastoma and rat neuronal cells were imaged with confocal microscopy

as changes in the red/green fluorescence intensity ratio. The significant decrease in the mean

red/green ratio observed in cells over-expressing the β-secretase BACE1, or the α-secretase

ADAM10, fused to a monomeric blue fluorescent protein confirms that the proteolytic site is still

accessible. Interestingly, we found that the degree of proteolytic processing of APP is not

completely homogeneous within the same single cell, and that there is a high degree of

variability between cells of the same type. We were also able to follow with a fluorescence

spectrometer the changes in the red emission intensity of the extracellular medium when

BACE1 was overexpressed. This represents a complementary approach to fluorescence

microscopy for rapidly detecting changes in the proteolytic processing of APP in real time. In

order to allow the discrimination between the α- and the β-secretase activity, we have created a

variant of mChAPPmGFP with a mutation that inhibits the α-secretase cleavage without

perturbing the β-secretase processing. Moreover, we obtained a quantitatively robust estimate

51   of the changes in the red/green ratio for all the above conditions by using a flow cytometer able

52   to simultaneously excite and measure the red and green fluorescence. Our novel approach lays

53   the foundation for a bioassay suitable to study the effect of drugs or particular conditions, to

54   investigate in an unbiased way the proteolytic processing of APP in single living cells, and to

55   elucidate the causes of the variability and the factors driving the processing of APP.

56

57

58

59

60

61

62

63

64

65

66

67

68

69

Introduction

In the last decades the incidence of Alzheimer's disease (AD) has risen due to an increase in

the lifespan, representing more and more a serious social problem. The first steps in the

pathological cascade involve protein quality control impairment and the failure of misfolded

proteins clearance mechanisms, with subsequent accumulation and oligomeritazion of

neurotoxic amyloid-β peptide. Aβ oligomers decrease the synaptic efficacy, activate microglia

and astrocytes causing an inflammatory response, alter the degree of tau's phosphorylation

leading to tangles, deposit in the brain blood vessels and cause neuronal loss and

neurotransmitter deficits(Selkoe and Hardy, 2016). The generation of amyloid-β peptide results

from the sequential cleavage of the amyloid precursor protein (APP) by β-secretase and γ-

secretase(Haass, 2004) (De Strooper, 2010). This process is in competition with an alternative

non-pathogenic pathway lead by the α-secretase(De Strooper, 2010). APP is a plasma

membrane glycoprotein whose original function remains unclear (Senechal, Larmet and Dev,

2006). The β-secretase and the other secretases have become obvious therapeutic targets for

drug research in AD (MacLeod, et al., 2015). Several strategies have mainly focused on the

inhibition of β-secretase and γ-secretase or, alternatively, on Aβ clearance. Unfortunately, none

of these pharmacological therapies has yet passed the phase II/III trial due to a lack of

encouraging results, or to the onset of adverse side effects (MacLeod, et al., 2015). Despite the

recent failures, significant hope still lies around the secretase targeting approach. With this

regard, the full understanding of the factors governing the rate of proteolytic processing of APP

is imperative. Commercial kits (Sigma-Aldrich, Abcam) to evaluate the activity of the β-

secretase BACE1 from human and animal samples are available. These assays use a specific

BACE1 substrate conjugated to two reporter molecules. In the uncleaved form, the fluorescence

of the reporter is quenched by the physical proximity of the other molecule. After the cleavage

by β-secretase, the two molecules are separated and a fluorescent signal can be acquired with

95 intensity proportional to the enzymatic activity. This type of kit is very efficient in detecting the

96 activity of BACE1 from purified samples, but remains an *in vitro* evaluation. By contrast, we

97 have developed a consistent bioassay to quantify in an unbiased way the the proteolytic

98 processing of APP in single living cells. The key element of our assay is a chimeric construct of

99 APP with two different fluorescent proteins fused at the opposite terminals. Changes in the

100 proteolytic processing of APP are seen as changes in the intensity ratio of the two fluorescent

101 protein tags. We demonstrate that our mChAPPmGFP construct is efficiently recognized and

102 cleaved by both α- and β-secretase. The activity of each individual secretase can be

103 discriminated by using specific siRNAs or, alternatively, by introducing specific mutations at the

104 cleavage sites of APP. Here, we have created a mutated variant of mChAPPmGFP that can be

105 cleaved almost exclusively by β-secretase (mChAPP^{P1}mGFP). The mutation, a Lys to Val

106 substitution at position 612 of APP695, just before the α-secretase cleavage site (this position is

107 called P1), has already been used to verify the sequence specificity of α-secretase

108 cleavage(Sisodia, 1992) . Sisodia tested a series of mutants at the P1 position, and found by

109 immunoprecipitation studies that only one, the Lys to Val substitution, prevents the α-secretase

110 cleavage.

111 Finally, we obtained a quantitatively robust validation of our bioassay by using a flow cytometer

112 able to simultaneously excite and measure the emission intensity of the two fluorescent

113 proteins.

114

115

Materials and Methods

116

Cloning

117

118   To generate the fusion constructs of mChAPPmGFP and mChAPP770mGFP we used

119   APP695 and APP770 contained in the vector pCMV-AC-GFP (Origene, Rockville MD, USA).

120   First, we inserted new restriction sites (NheI, AscI) after the signal peptide using the GeneArt

121   Site-Directed Mutagenesis Kit (ThermoFisher Scientific), using

122   GCCGCCTGGACGGCTCGGGCGGCTAGCCAGGGCGCGCCTCTGGAGGTACCCACTGATG

123   G as forward primer, and

124   CCATCAGTGGGTACCTCCAGAGGCGCGCCCTGGCTAGCCGCCCGAGCCGTCCAGGCGGC

125   as reverse primer. The mCherry sequence was amplified from its original plasmid (pmCherry-C1

126   vector, Clontech) with a PCR reaction (forward primer:

127   TAAGCAGCTAGCATGGTGAGCAAGGGCGAGGAG, reverse primer

128   TGGCGCGCCTGTTCCACGACTCTTGTACAGCTCGTCCATG) adding the restriction

129   sequences for the enzymes NheI and AscI. After digestion, the sequence of mCherry was

130   inserted at the N-term of APP. In order to substitute the dimerizing TurboGFP present in the

131   pCMV-AC-GFP vector with the monomeric green fluorescent protein mTagGFP2, mCherry-

132   APP695 and mCherry-APP770 were excised from their original plasmid using the restriction

133   enzymes SgfI and NotI and inserted in the plasmid pCMV6-AN-mGFP (commercial name of

134   mTagGFP2, Origene) to obtain the final fusion constructs mCherry-APP695-mGFP and

135   mCherry-APP770-mGFP. The QuikChange Lightning Site-Directed Mutagenesis Kit (Agilent)

136   was used to mutagenize the mChAPPmGFP construct in order to create a new plasmid

137   (mChAPP[P1]mGFP) carrying the P1 mutation, a Lys to Val substitution at P1 position (amino

138   acid 612 of APP695), that is the amino acid located before the α-secretase cleavage

139   site(Sisodia, 1992) (forward primer: GAAGTTCATCATCAAGTATTGGTGTTCTTTGC, reverse

140   primer: GCAAAGAACACCAATACTTGATGATGAACTTC).

141   To generate the fusion construct Bace1-mBFP and HA-Bace1-mBFP, we started from Bace1

142   contained in the vector pCMV6-ENTRY (NM_012104, Origene, Rockville, MD, USA). We

143   opened the vector using the restriction enzymes NotI and SacII. mBFP (original name

144   mTagBFP2) was extracted with a PCR reaction from the plasmid pmTagBFP2-N1(Subach, et

145   al., 2011) (forward primer: TAAGCAGCGGCCGCGAATGAGCGAGCTGATTAAGG, reverse

146   primer: CCGAGTCCGCGGTTAATTAAGCTTGTGCCCCAG) to add the restriction sequences of

147   the enzymes NotI and SacII. After digestion, the sequence of mBFP was inserted in the plasmid

148   of Bace1 previously opened with the same enzymes, to obtain the final fusion construct Bace1-

149   mBFP. With a site-directed mutagenesis reaction (ThermoFisher Scientific) we added the

150   restriction sites for NheI and AscI at the N-term of Bace1-mBFP (forward primer:

151   GGAGTGCTGCCTGCCCACGGCGCTAGCCAGGGCGCGCCtACCCAGCACGGCATCCGGCT

152   G, reverse primer

153   CAGCCGGATGCCGTGCTGGGTAGGCGCGCCCTGGCTAGCGCCGTGGGCAGGCAGCACT

154   CC). We opened the plasmid of Bace1-mBFP and inserted the annealed oligos containing the

155   sequence for the HA tag (forward oligo: CTAGCTATCCGTACGACGTACCAGACTACGCAGG,

156   reverse oligo: CGCGCCTGCGTAGTCTGGTACGTCGTACGGATAG). After ligation we obtained

157   the plasmid of the construct HA-Bace1-mBFP.

158   ADAM10mBFP was created by the fusion of the mTagBFP2 gene downstream of the ADAM10

159   gene contained in the pRK5M-ADAM10 construct (Addgene). The final part of the sequence

160   coding for ADAM10 was mutagenized in order to introduce two new restriction sites, unique

161   within the entire sequence of the plasmid. The site-directed mutagenesis was performed with

162   the QuikChange Lightning Site-Directed Mutagenesis Kit (Agilent Technologies), using

163   GAGGACCTGCTGCGTACGGTCGCGCGCGCTTGGCCGCCA as forward primer and

164   TGGCGGCCAAGCGCGCGCGACCGTACGCAGCAGGTCCTC as reverse primer, containing

165   the restriction sequences for the BsiWI e BssHII enzymes. The mTagBFP2 sequence was

NOT PEER-REVIEWED

166   amplified from its original plasmid (pmTagBFP2-N1, Addgene) with a PCR reaction (forward

167   primer GAGCGTACGATGAGCGAGCTGATTAAGGAG, reverse primer

168   GTAGCGCGCTTAATTAAGCTTGTGCCCCAG, the forward primer containing the BsiWI

169   restriction site and the reverse the BssHII one). After digestion, the sequence of BFP2 was

170   inserted at the C-terminal of ADAM10.

171   apAPPha was created from mChAPPmGFP using the restriction sites for NheI and AscI at the

172   N-term. First, we opened the plasmid with these enzymes and inserted the annealed oligos

173   containing the sequence for the genetic tag AP (forward oligo:

174   CTAGCGAGGGCCTGAACGATATCTTCGAGGCCCAGAAGATCGAGTGGCACGAGAGTGGre

175   verse oligo:

176   CGCGCCACTCTCGTGCCACTCGATCTTCTGGGCCTCGAAGATATCGTTCAGGCCCTCG).

177   Afterwards, we opened the plasmid with the restriction enzimes NotI and SacII in order to

178   substitute mGFP with the annealed oligos containing the sequence for the genetic tag HA

179   (forward oligo:

180   GGCCGCTCGAGTATCCGTACGACGTACCAGACTACGCAGTTTAAACCCGC,

181   reverse oligo: GGGTTTAAACTGCGTAGTCTGGTACGTCGTACGGATACTCGAGC).

Cell cultures and transfection

183   Human SH-SY5Y neuroblastoma cells (A.T.C.C. Manassas, VA, USA) were cultured in

184   Dulbecco's Modified Eagle's Medium (DMEM) F-12 supplemented with 10% FBS, 1%

185   penicillin/streptomycin solution. HEK cells were cultured in DMEM Glutamax supplemented with

186   10% FBS, 1% penicillin/streptomycin solution. Primary rat hippocampal neurons were obtained

187   after dissociation of hippocampi purchased from Brainbits, UK. Neurons were plated on

188   coverslips coated with poly-L-ornithine and grown in Neurobasal medium supplemented with 2%

189   B27, 0,5 mM glutamine, 12,5 mM glutamate and 0,1 % penicillin/streptomycin. All the cell types

190   were cultured in a humidified chamber at 5% CO_2 and 37°C. Neuroblastoma SH-SY5Y cells

191   were transfected with Fugene HD (Promega, USA) 24-48 h before imaging. HEK cells were

192   transfected with Lipofectamine 2000 (ThermoFisher Scientific) 24-48 h before imaging. To

193   transfect hippocampal neurons DNA was mixed with Lipofectamine 2000 in 0,5 ml of

194   Neurobasal supplemented with 0,5 mM glutamine at 37°C in 5% CO_2 for 60 min. Afterwards

195   neurons were rinsed with Neurobasal, transferred to the original medium at 37 °C 5% CO_2 and

196   imaged after 24-48 h. apAPPha was co-transected with BirA, a biotin ligase that specifically

197   biotinylates the AP tag . Biotin was added to the cell medium (final concentration 10 μM) 8 hours

198   after transfection and 12 hours before imaging(Howarth, et al., 2005). siRNA Silencer®

199   Validated siRNA against BACE1 (105154) and *Silencer*® Negative Control siRNA were

200   purchased from ThermoFisher. Supplementary Figure S5 shows the silencing efficiency of

201   Bace1-siRNA.

Cell imaging

203   Live cell imaging was performed on a Nikon Eclipse TE300 C2 LSCM (Nikon, Japan) equipped

204   with a Nikon 60x immersion oil objective (Apo Plan, NA 1.4). Cells were growth on 18 mm

205   coverslips and mounted on a custom chamber containing 1 ml of Leibovitz's medium

206   (ThermoFisher). For immunolabelling, cells were fixed with 4% PFA, rinsed with PBS (+$MgCl_2$

207   0,5 mM, +$CaCl_2$ 0,8 mM) and permeabilized with 0,075% Triton X. After rinsing with PBS and

208   blocking with 4% BSA PBS, cells were labelled with primary (1:1000 rabbit anti-HA ab9110 -

209   Abcam, UK-) and secondary antibodies (goat anti-rabbit Alexa 488,–ThermoFisher, diluted at

210   1:500), or streptavidin Alexa 568 (ThermoFisher diluted at 1:500), diluted in PBS with 4% BSA.

211   After rinsing again with PBS, coverslips were mounted on a glass slide and imaged with LSCM,

212   equipped with Coherent CUBE (diode 405 nm), Melles Griot (Argon 488 nm) and Coherent

213   Sapphire (Sapphire 561 nm) lasers. Emission filters for imaging were 452/45 nm, 514/30 nm

214   and 595/60 nm. For surface labeling, living SH-SY5Y cells were growth on 18 mm coverslips,

215   rinsed with PBS and incubated with primary antibodies (1:100 rabbit anti-mCherry ab167453, or

216   1:1000 rabbit anti-HA ab9110 -Abcam, UK-) diluted in PBS with 4% BSA for 30 minutes on ice,

217   to inhibit endocytic events. After rinsing with PBS,cells were incubated with secondary

218   antibodies (1:500 goat anti-rabbit Alexa 405) diluted in PBS with 4%BSA for 15 minutes. After

219   rinsing again the coverslips, cells were mounted on a custom chamber filled with Leibovitz's

220   medium and imaged with the same LSCM configuration mentioned above.

Western blotting

222   Human SH-SY5Y neuroblastoma cells were cultured in 6 wells plates. 24 h after transfection,

223   the extracellular medium was recovered and the cells were lysed using 300 µl of PBS and

224   Laemmli buffer. Lysed cells were collected in safe lock 1,5 ml tubes and immersed in boiling

225   water for 5 minutes, then sonicated two times for 15 seconds and boiled again for 5 minutes.

226   The recovered medium was centrifuged at 10000 rpm for 5 min in order to remove cell debrees

227   and other impurity, and then treated as the cell lysate. Samples were loaded in pre-casted

228   polyacrylamide gels (ThermoFisher Scientific, MA USA) and blotted on PVDF membranes

229   (ThermoFisher Sicnetific, MA USA). Membranes were blocked in 5% milk in PBST overnight at

230   4°C or 1 h at room temperature. After blocking, membranes were rinsed three times with PBST

231   and incubated at room temperature with primary antibody (in PBST with 4% BSA) for 1 h and for

232   an additional hour with secondary anti-rabbit antibody conjugated to horseradish peroxidase

233   (1:20000). The primary antibodies were: rabbit anti-mCherry (1:1000, Abcam, UK, ab167453),

234   rabbit anti-APP (1:200, Abcam ab15272), rabbit anti-vimentin (1:2500, Abcam ab92547

235   EPR3776) mouse anti-aβ (1:100, Abcam ab11132 DE2b4), mouse anti-GFP (1:1000 Abcam,

236   ab291 LGB-1). Membranes were rinsed with the HRP substrate Pico Dura (ThermoFisher

237   Scientific, MA USA) and imaged after 5 min with a Chemidoc MP system (Bio-Rad, CA USA). In

238   order to perform the stripping procedure, the blotted PVDF membranes were covered with

239   Seppro Stripping Buffer (Sigma Aldrich, MO USA) and incubated for 5-10 min at room

240   temperature. The stripping buffer was then discarded and the incubation was repeated with

241　fresh Seppro buffer for 5-10 min. After discarding the buffer, membranes were washed for two

242　times with PBS for 10 minutes, then washed for two times with TBST for 5 minutes and blocked.

Fluorescence spectroscopy

244　Fluorescence spectra from 585 nm to 700 nm were acquired at 25 °C in a 10 ×10 mm quartz

245　cuvette using a Perkin-Elmer LS 55 spectrofluorimeter (Waltham, MA, USA) equipped with a

246　thermostated cell holder attached to a Haake F8 water bath (Karlsruhe, Germany). Excitation

247　wavelength was 550 nm.

FACS

249　Cells were harvested after mild trypsin treatment and centrifuged for 5 min at 330 g; the

250　obtained pellets were washed and re-suspended in PBS. We cannot exclude that the treatment

251　with trypsin might affect the integrity of the ectodomain of mChAPPmGFP; however, all the

252　conditions of transfection tested would have been affected equally without influencing the

253　conclusion of our experiments. Flow cytometry was performed by using a S3 flow cytometer

254　(Bio-Rad) equipped with 488 and 561 nm diode-pumped solid-state lasers. mGFP was excited

255　using the 488 nm laser, and the emitted fluorescence was collected through a 586/25 nm band-

256　pass filter; mCherry was excited with the 561 nm laser and its fluorescence was collected

257　through a 615/25 nm band-pass filter. Data were analysed using *ProSort* software (Bio-Rad), by

258　dividing the scatter plot of mGFP versus mCherry into two equally populated regions under

259　control conditions. The cellular debris was excluded from the quantification by gating cells on

260　the Forward scatter area/Side scatter area (FSC/SSC) graph, while doublets were excluded by

261　gating the cells on the Forward scatter height/ Forward scatter area (FSC/FSC) graph; at least

262　10000 events were acquired for each sample.

263

264 # Results

265 ## mChAPPmGFP is correctly targeted to the plasma

266 ## membrane

267 APP695, the isoform mainly expressed in the central nervous system (Nalivaeva and Turner,

268 2013), was fused to a monomeric variant of the green fluorescent protein (mGFP) at the C-

269 terminal and to a monomeric red fluorescent protein (mCherry) at the N-terminal (Fig. 1). In this

270 way the extremities of APP situated at the opposite sides of the plasma membrane are labeled

271 with two different fluorescent proteins. Once the N-term mCherry containing domain is cleaved,

272 the fluorescence intensity ratio between the red and green signals changes. It is thus possible to

273 monitor in living cells a higher or lower processing of APP in function of the ratio shift. From

274 herein, we will refer to this chimeric construct bearing the APP695 isoform as to

275 mChAPPmGFP. The same procedure was repeated to obtain the fusion construct of APP770

276 (mChAPP770mGFP), an alternative isoform expressed more ubiquitously (Zheng and Koo,

277 2011).

278 mCherry was fused immediately after the signal peptide, which is necessary to target APP to

279 the plasma membrane, and away from the site recognized and cleaved by the β-secretase . In

280 order to test if mChAPPmGFP is correctly targeted to the plasma membrane, we performed a

281 surface immunolabelling of transfected human SH-SY5Y neuroblastoma cells with a primary

282 anti-mCherry antibody (Fig. 2a). Confocal laser scanning microscopy (CLSM) imaging reveals a

283 good degree of labeling only in cells expressing mChAPPmGFP, confirming that mCherry is

284 correctly folded and present on the surface of the cell. We observed red clusters not colocalising

285 with anti-mCherry, thus indicating their intracellular localization.

286   To confirm that the full-length chimeric mChAPPmGFP protein was expressed, we examined

287   the colocalization of mCherry and mGFP in neuroblastoma cells (Fig. 2 b-d) and rat

288   hippocampal neurons (Fig. 2 e-g). The toolbox available with the JACoP plug-in(Bolte and

289   Cordelieres, 2006) under the ImageJ software(Schneider, Rasband and Eliceiri, 2012) was used

290   to quantify the degree of colocalization . We found that in most cells the plot of the pixel intensity

291   of the green against that of the red channel (scatterplot) follows a linear relationship, with an

292   average Pearson's coefficient (an estimate of the quality of the linear relationship between the

293   two signals with 1 standing for complete positive correlation) of 0.91. We also found an average

294   Manders' overlap coefficient(Manders, et al., 1992) M1 (indicating the fraction of mCherry

295   overlapping with mGFP) of 0.97 and an M2 (fraction of mGFP overlapping mCherry) of 0.85.

296   The measured Costes' randomization P-value(Costes, et al., 2004) of 100% excludes that the

297   co-localization of pixels is due to chance. An additional method such as Li's intensity correlation

298   analysis(Li, et al., 2004) further supports a very good degree of   colocalization, indicating an

299   abundant presence of full-length mChAPPmGFP. We recurrently observed small red fluorescent

300   punctae, at which did not correspond a comparable level of green fluorescence intensity. Similar

301   data were obtained for mChAPP770mGFP (Supplementary Fig. S1).

302   Due to their size and consequent steric hindrance, the two fluorescent tags could alter the

303   distribution features of APP. However, we did not observe any significant difference in the

304   overall cellular distribution after immunolabeling of an overexpressed construct of APP695

305   bearing two small tags (AP(Howarth, et al., 2005) and HA(Schembri, et al., 2007), apAPPha) at

306   the two opposite terminals (Fig. 2h-j). As previously reported(Collins, et al., 2010;Guo, et al.,

307   2012;Haass, et al., 2012), a large fraction of intracellular mChAPPmGFP is localized at the level

308   of the Golgi apparatus, in the perinuclear region (Supplementary Fig. S2). In agreement with an

309   elegant study investigating the subcellular localization of endogenous full length APP in

310   neurons(Guo, et al., 2012), mChAPPmGFP also shows partial co-localization with the

311   endoplasmic reticulum, but very little with early endosomes and lysosomes (Supplementary Fig.

312   S2). We find this study of particular relevance since it shows with a knock-out model that many

313   antibodies against APP commonly used for immunofluorescence experiments give rise to non-

314   specific labeling.

Fluorescence intensity ratio heterogeneity

316   We then measured the ratio between the red and the green fluorescence intensity in

317   neuroblastoma cells (Fig. 3 a) and rat hippocampal neurons (Fig. 3 b). The ratio image was

318   generated using the Ratio Plus available on ImageJ (Schneider, et al., 2012). Regions of

319   interest (ROIs) for the calculation of the mean ratio value per cell were chosen by using a

320   constant threshold value on the maximum projection of mGFP stacks. The ROIs were then

321   applied to the corresponding ratio image. The gain used for the acquisition of neuronal images

322   was different from that of neuroblastoma cells due to differences in the level of protein

323   expression. We observed a certain degree of intracellular heterogeneity in the red/green ratio,

324   with lower red/green ratio in the peripheral areas of the cells. In addition, we observed a

325   relatively high intercellular variability among the same population of transfected neuronal or

326   neuroblastoma cells.

327

mChAPPmGFP is cleavable by Bace1

329   In order to check if our fusion protein was correctly folded, recognized and cleaved, we co-

330   transfected SH-SY5Y (Fig. 4) and neuronal cells (Fig. 5) with mChAPPmGFP together with β-

331   secretase Bace1 fused with mTagBFP2 (mBFP) at the C-term. We found that overexpressed

332   BACE1 is aboundantly present on the plasma membrane (Supplementary Fig. S3). When

333   Bace1-mBFP cleaves mChAPPmGFP on the cell surface, the soluble fragment mCherry-sAPPβ

334   is released in the extracellular medium. We compared the mean red/green ratio in cells

335   expressing mChAPPmGFP with or without Bace1-mBFP (Fig. 4 a-c; Fig. 5). While we did not

336   find statistically significant differences in cells transfected with siRNA against Bace1 (although

337   an unpredicted minor reduction in the ratio is visible), the overexpression of Bace1-mBFP

338   dramatically decreased the ratio. Although APP might undergo a major processing by α-

339   secretase under physiological conditions, the contribution of the latter is negligible when APP is

340   overexpressed with BACE1. Cells transfected with mChAPP770mGFP showed a comparable

341   trend.

342   Equivalent results were obtained when performing western blots of both cell lysate and

343   extracellular medium of SH-SY5Y cells co-transfected with mChAPPmGFP and Bace1-mBFP or

344   Bace1-siRNA, using anti-mCherry as primary antibody for chemoluminescent detection (Fig.

345   4d). In the lysate of cells co-transfected with mChAPPmGFP and Bace1-siRNA, two bands were

346   detected, one more intense at 152 KDa, corresponding to full-length mChAPPmGFP (expected

347   molecular weight 134 KDa), and one at 125 KDa, possibly corresponding to mCherry-sAPPα

348   (expected molecular weight 100 KDa) generated by endogenous α-secretase. For cells co-

349   transfected with mChAPPmGFP and Bace1-mBFP, the same two bands were visible, but in this

350   case the lower band was more intense, due to an increased production of mCherry-sAPPβ,

351   which has a molecular weight (expected molecular weight 94 KDa) comparable to mCherry-

352   sAPPα. Blotting of the extracellular medium revealed only one band at 121 KDa, corresponding

353   to the released mCherry-sAPPfragment. A considerably higher intensity band was found in the

354   case of cells co-transfected with Bace1 (increased production of mCherry-sAPPβ) as compared

355   to those co-transfected with Bace1-siRNA (mostly mCherry-sAPPα). Analogous results were

356   obtained for the cell lysate and the extracellular medium of cells transfected with

357   mChAPP770mGFP, with the bands being at higher molecular weights: ~163 KDa for the

358   uncleaved mChAPP770mGFP (expected molecular weight 142 KDa) and ~138 KDa for the

359   mCherry-sAPP770β (expected molecular weight 102 KDa).

360 Membrane stripping and reprobing with anti-GFP, anti-APP (directed against the N-terminal 44-

361 62 amino acids) or anti-Aβ (directed against amino acids 1-17 of Aβ) generated analogous

362 results. At long time exposures of the blot, bands corresponding to the C-terminal fragments of

363 mChAPPmGFP (C83/89-mGFP and AICD-mGFP) are visible (Supplementary Fig. S4). These

364 data corroborate further that our construct is recognized and processed by BACE1.

365 Furthermore, we collected and analyzed the supernatant media from different transfection

366 conditions of SH-SY5Y cells with a fluorescence spectrophotometer. In agreement with the

367 above results, we observed higher fluorescence intensity at 610 nm (maximum emission peak

368 for mCherry) in cells co-expressing mChAPPmGFP together with Bace1-mBFP (Fig. 4 e). This

369 result further supports that β-secretase recognizes and cleaves our fusion APP construct, which

370 is then in part released in the extracellular medium as mCherry-sAPPβ. Similar results were

371 found in HEK cells (Supplementary Fig. S5). Our data show an unexpected slight increase in

372 fluorescence intensity at 610 nm in the cells co-transfected with Bace1-siRNA compared to the

373 control condition. Overall these results suggest that the site cleaved by β-secretase is still

374 accessible and that is possible to follow the processing of APP as function of the ratio shift.

375 We finally validated our results with FACS flow cytometry, a statistically robust technique

376 capable of analyzing the red and green fluorescence intensity for a large number of single cells.

377 SH-SY5Y cells were co-transfected with mChAPPmGFP and Bace1-mBFP, or control siRNA, or

378 Bace1-siRNA. Two different areas in the red versus green fluorescence scatter plot were

379 arbitrarily chosen so that both areas contained the same number of cells co-transfected with

380 mChAPPmGFP and control siRNA (Fig. 6). The overexpression of Bace1-mBFP changed

381 significantly the ratio between the number of cells in the red and green areas. We observed only

382 a slight, although not significant, increase in the ratio when cells were co-transfected with siRNA

383 directed against Bace1. Comparable results were found using HEK cells (Supplementary Fig.

384 S6).

385

The P1 mutation inhibits the processing of APP by ADAM10

387   SH-SY5Y neuroblastoma cells were co-transfected with mChAPPmGFP or mChAPP^{P1}mGFP

388   and ADAM10mBFP in order to test whether the P1 mutation really inhibits the α-secretase

389   activity. We compared the mean red/green ratio in cells overexpressing ADAM10mBFP and

390   mChAPPmGFP with or without the P1 mutation (Fig. 7a-b). The red/green ratio was found to be

391   significantly higher in cells overexpressing mChAPP^{P1}mGFP compared to mChAPPmGFP,

392   showing not only that the ADAM10mBFP construct is proteolytically active, but also that the

393   presence of the P1 mutation strongly prevents the cleavage by α-secretase. These results were

394   validated by FACS flow cytometry (Fig. 7c and Fig S7). SH-SY5Y cells were co-transfected with

395   mChAPPmGFP or mChAPP^{P1}mGFP and ADAM10mBFP or mBFP. As above, two different

396   areas containing the same number of cells co-transfected with mChAPPmGFP and mBFP were

397   used to gate the scatter plots of cells co-transfected with the other conditions and calculate the

398   mean ratio between the number of cells in the red area over the number of cells in the green

399   area. The number of cells in the red area significantly increased with the overexpression of

400   mChAPP^{P1}mGFP compared to the wild-type, both in the presence of ADAM10mBFP or mBFP,

401   denoting an almost complete resistance to α-secretase proteolysis. Moreover, SH-SY5Y cells

402   were co-transfected with mChAPP^{P1}mGFP and BACE1mBFP in order to verify potential side-

403   effects of the P1 mutation on the β-secretase processing. The ratio between the number of cells

404   in the red and green areas resulting from the co-expression of mChAPP^{P1}mGFP and

405   BACE1mBFP is comparable with that from mChAPPmGFP and BACE1mBFP. This data

406   suggests that the variant of APP carrying the P1 mutation is hardly processed by ADAM10,

407   while still cleavable by Bace1.

408

Discussion

409

410   We have successfully demonstrated the proof of principle of a bioassay to evaluate the

411   processing of APP directly in single living cells, a less biased method compared to the *in vitro*

412   kits that are commercially available. To estimate the rate of processing of APP, we measured

413   the variation in the red/green fluorescence ratio emitted from cells overexpressing

414   mChAPPmGFP. We demonstrated that mChAPPmGFP is correctly folded and targeted to the

415   plasma membrane, and it is still cleavable by the β-secretase Bace1. We have noticed that a

416   similar approach has been tested in two previous works(Coughlan, et al., 2013;Villegas,

417   Muresan and Ladescu Muresan, 2014). In one of these papers, the residual C-terminal region of

418   APP770 (106 amino acids) carrying the Swedish mutation was fused with two different

419   fluorescent proteins (DsRed2 and EGFP) at the opposite terminal sides(Coughlan, et al., 2013).

420   By contrast, our mChAPPmGFP construct is generated from the full length APP695 and

421   contains the original signal-peptide sequence that is required for targeting the newly

422   synthesized protein to the plasma membrane. Furthermore, in order to avoid oligomerization

423   events, we used two monomeric fluorescent proteins, mCherry and mGFP. These two

424   fluorescent proteins have comparable maturation times of approximately 10-15 minutes(Shaner,

425   et al., 2004;Subach, et al., 2008), thus limiting the rise of artifacts due to different maturation

426   events. In agreement with the fact that the mCherry and the mGFP tags are kept more than 10

427   nm apart by the plasma membrane, we did not observe any Foster resonance energy transfer

428   (FRET), preserving therefore the linearity of the red/green ratio with respect of the amount of

429   cleaved APP (Supplementary Fig. S8). In the other interesting work(Villegas, et al., 2014),

430   APP695 was fused to CFP and YFP at the two opposite terminals, with CFP correctly positioned

431   after the signal peptide, to study the localization of APP fragments and the trafficking processes

432   occurring intracellularly. The authors found that the presence of the tags did not alter the

433   processing of APP by the secretases, and that some intracellular N-terminal fragments –

434   possibly corresponding to our observed red punctae - do not colocalize with full length APP or

435   C-terminal fragments, in complete agreement with our data. Importantly, the dual tagged APP,

436   at low level of expression, showed a subcellular distribution and a proteolytical profile highly

437   comparable to that of endogenous APP.

438   Interestingly, our results show that cells of the same type (both neuronal and neuroblastoma

439   cells) display different ratios of red/green fluorescence intensity, suggesting that the processing

440   rate of APP is highly variable even within the same population. Furthermore, a certain level of

441   heterogeneity in the red/green intensity ratio is also found within the same cell, indicating that

442   the activity of the proteases can vary in different districts of the cell. This finding is in agreement

443   with previous results showing that there are differences in the processing of APP depending on

444   its targeting on the plasma membrane of highly polarized cells (Haass, et al., 2012) (DeBoer, et

445   al., 2014)**.**

446   It has been shown that APP can be internalized from the cell surface and specifically targeted to

447   lysosomes(Tang, et al., 2015). Previous works demonstrated that the fluorescence emitted by

448   GFP can be strongly reduced by the acidic pH of the lysosomal lumen, while the fluorescence

449   emitted by mCherry remains stable in a broad range of pH (Katayama, et al., 2008;Mizushima,

450   Yoshimori and Levine, 2010). These considerations could in part explain the presence in our

451   images of intracellular vesicles with high red fluorescence intensity barely co-localizing with the

452   green fluorescence signal. However, the fact that we did not observe any co-localization with

453   the lysosome marker LAMP1 does not convincingly support this hypothesis. It is rather plausible

454   that the red punctae correspond to cleaved N-terminal fragments transported in vesicles

455   separated from those carrying the full length protein and the C-terminal fragments, as already

456   observed by Villegas et al. (2014).

457   As an alternative to the siRNAs, we have created a variant of mChAPPmGFP carrying a

458   mutation capable of inhibiting the α-secretase processing without altering the β-secretase

459 cleavage. The importance of this construct is the possibility to create transgenic animals, like

460 zebra-fish and rat, which could be used to produce a 3D map of the whole brain showing areas

461 with potentially different β-secretase activities. Previous data(Sisodia, 1992), together with our

462 confocal microscopy and FACS results, suggest that the P1 mutation makes APP cleavage-

463 resistant by α-secretase. However, it is unclear whether it completely inhibits the APP

464 processing. Although cells co-transfected with ADAM10mBFP and mChAPP^{P1}mGFP have a cell

465 number in the red/green area ratio similar to that of cells co-expressing mBFP and

466 mChAPPmGFP, the ratio for mBFP and mChAPP^{P1}mGFP transfected cells is much higher than

467 the ratio for ADAM10mBFP and mChAPP^{P1}mGFP transfected cells. It is possible that under

468 conditions where ADAM10 is strongly overexpressed, a small fraction of mChAPP^{P1}mGFP can

469 be still cleaved.

470 In general, FACS flow cytometry corroborated the reliability of our bioassay and confirmed the

471 heterogeneous processing of APP within the same type of cells. Furthermore, the possibility to

472 separate cells with different rates of APP processing, i.e. different red/green ratios, using the

473 cell-sorting capability of FACS might allow to perform a complete proteomic, lipidomic and

474 transcriptomic analysis of these sub-populations of cells, and to address one of the most

475 puzzling questions in the context of Alzheimer's disease: why the proteolytic processing of APP

476 is higher in certain cells than in others.

477 The combined approach presented in this work could be also used as versatile bioassay to test

478 in living cells the effect of specific molecules on the proteolysis of APP. A more detailed

479 knowledge of the factors governing the processing of APP could contribute to develop

480 alternative drugs for AD treatments.

481

Acknowledgements

482

483 We thank Dr. Francesco Bemporad, Dr. Daniele Nosi, Dr. Franco Quercioli and Rachele

484 Raggioli for their technical help.

485

486

487

488

489

490

491

492

493

494

495

496

497

498

499

500

501

502

503

504

505

506

507

508

References

510   Bolte, S. & Cordelieres, F. P. (2006) A guided tour into subcellular colocalization
511   analysis in light microscopy. *Journal of microscopy* 224, 213-232, doi:10.1111/j.1365-
512   2818.2006.01706.x.

513   Collins, A. J., Foley, R. N., Herzog, C., Chavers, B. M., Gilbertson, D., Ishani, A.,
514   Kasiske, B. L., Liu, J., Mau, L. W., McBean, M., Murray, A., St Peter, W., Guo, H., Li, Q.,
515   Li, S., Li, S., Peng, Y., Qiu, Y., Roberts, T., Skeans, M., Snyder, J., Solid, C., Wang, C.,
516   Weinhandl, E., Zaun, D., Arko, C., Chen, S. C., Dalleska, F., Daniels, F., Dunning, S.,
517   Ebben, J., Frazier, E., Hanzlik, C., Johnson, R., Sheets, D., Wang, X., Forrest, B.,
518   Constantini, E., Everson, S., Eggers, P. W. & Agodoa, L. (2010) Excerpts from the US
519   Renal Data System 2009 Annual Data Report. *American journal of kidney diseases : the*
520   *official journal of the National Kidney Foundation* 55, S1-420, A426-427,
521   doi:10.1053/j.ajkd.2009.10.009.

522   Costes, S. V., Daelemans, D., Cho, E. H., Dobbin, Z., Pavlakis, G. & Lockett, S. (2004)
523   Automatic and quantitative measurement of protein-protein colocalization in live cells.
524   *Biophysical journal* 86, 3993-4003, doi:10.1529/biophysj.103.038422.

525   Coughlan, K., Huang, X., He, X., Chung, C. H., Li, G. & Tang, J. (2013) Expression and
526   processing of fluorescent fusion proteins of amyloid precursor protein (APP). *Biochimica*
527   *et biophysica acta* 1833, 1562-1571, doi:10.1016/j.bbamcr.2013.03.003.

528   De Strooper, B. (2010) Proteases and proteolysis in Alzheimer disease: a multifactorial
529   view on the disease process. *Physiological reviews* 90, 465-494,
530   doi:10.1152/physrev.00023.2009.

531   DeBoer, S. R., Dolios, G., Wang, R. & Sisodia, S. S. (2014) Differential release of beta-
532   amyloid from dendrite- versus axon-targeted APP. *The Journal of neuroscience : the*
533   *official journal of the Society for Neuroscience* 34, 12313-12327,
534   doi:10.1523/JNEUROSCI.2255-14.2014.

535   Guo, Q., Li, H., Gaddam, S. S., Justice, N. J., Robertson, C. S. & Zheng, H. (2012)
536   Amyloid precursor protein revisited: neuron-specific expression and highly stable nature
537   of soluble derivatives. *The Journal of biological chemistry* 287, 2437-2445,
538   doi:10.1074/jbc.M111.315051.

539   Haass, C. (2004) Take five--BACE and the gamma-secretase quartet conduct
540   Alzheimer's amyloid beta-peptide generation. *The EMBO journal* 23, 483-488,
541   doi:10.1038/sj.emboj.7600061.

542   Haass, C., Kaether, C., Thinakaran, G. & Sisodia, S. (2012) Trafficking and proteolytic
543   processing of APP. *Cold Spring Harbor perspectives in medicine* 2, a006270,
544   doi:10.1101/cshperspect.a006270.

545   Howarth, M., Takao, K., Hayashi, Y. & Ting, A. Y. (2005) Targeting quantum dots to
546   surface proteins in living cells with biotin ligase. *Proceedings of the National Academy of*
547   *Sciences of the United States of America* 102, 7583-7588,
548   doi:10.1073/pnas.0503125102.

549   Katayama, H., Yamamoto, A., Mizushima, N., Yoshimori, T. & Miyawaki, A. (2008) GFP-
550   like proteins stably accumulate in lysosomes. *Cell structure and function* 33, 1-12.

551   Li, Q., Lau, A., Morris, T. J., Guo, L., Fordyce, C. B. & Stanley, E. F. (2004) A syntaxin
552   1, Galpha(o), and N-type calcium channel complex at a presynaptic nerve terminal:
553   analysis by quantitative immunocolocalization. *The Journal of neuroscience : the official*
554   *journal of the Society for Neuroscience* 24, 4070-4081, doi:10.1523/JNEUROSCI.0346-
555   04.2004.

556   MacLeod, R., Hillert, E., Cameron, R. T. & Baillie, G. S. (2015) The role and therapeutic
557   targeting of α-, β- and γ-secretase in Alzheimer's disease. *Future Science O A* 1.

558   Manders, E. M., Stap, J., Brakenhoff, G. J., van Driel, R. & Aten, J. A. (1992) Dynamics
559   of three-dimensional replication patterns during the S-phase, analysed by double
560   labelling of DNA and confocal microscopy. *Journal of cell science* 103 (Pt 3), 857-862.

561   Mizushima, N., Yoshimori, T. & Levine, B. (2010) Methods in mammalian autophagy
562   research. *Cell* 140, 313-326, doi:10.1016/j.cell.2010.01.028.

563   Nalivaeva, N. N. & Turner, A. J. (2013) The amyloid precursor protein: a biochemical
564   enigma in brain development, function and disease. *FEBS letters* 587, 2046-2054,
565   doi:10.1016/j.febslet.2013.05.010.

566   Schembri, L., Dalibart, R., Tomasello, F., Legembre, P., Ichas, F. & De Giorgi, F. (2007)
567   The HA tag is cleaved and loses immunoreactivity during apoptosis. *Nature methods* 4,
568   107-108, doi:10.1038/nmeth0207-107.

569   Schneider, C. A., Rasband, W. S. & Eliceiri, K. W. (2012) NIH Image to ImageJ: 25
570   years of image analysis. *Nature methods* 9, 671-675.

571   Selkoe, D. J. & Hardy, J. (2016) The amyloid hypothesis of Alzheimer's disease at 25
572   years. *EMBO molecular medicine*, doi:10.15252/emmm.201606210.

573   Senechal, Y., Larmet, Y. & Dev, K. K. (2006) Unraveling in vivo functions of amyloid
574   precursor protein: insights from knockout and knockdown studies. *Neuro-degenerative*
575   *diseases* 3, 134-147, doi:10.1159/000094772.

576   Shaner, N. C., Campbell, R. E., Steinbach, P. A., Giepmans, B. N., Palmer, A. E. &
577   Tsien, R. Y. (2004) Improved monomeric red, orange and yellow fluorescent proteins
578   derived from Discosoma sp. red fluorescent protein. *Nature biotechnology* 22, 1567-
579   1572, doi:10.1038/nbt1037.

580   Sisodia, S. S. (1992) Beta-amyloid precursor protein cleavage by a membrane-bound
581   protease. *Proceedings of the National Academy of Sciences of the United States of*
582   *America* 89, 6075-6079.

583   Subach, O. M., Gundorov, I. S., Yoshimura, M., Subach, F. V., Zhang, J., Gruenwald, D.,
584   Souslova, E. A., Chudakov, D. M. & Verkhusha, V. V. (2008) Conversion of red
585   fluorescent protein into a bright blue probe. *Chemistry & biology* 15, 1116-1124,
586   doi:10.1016/j.chembiol.2008.08.006.

587   Subach, O. M., Cranfill, P. J., Davidson, M. W. & Verkhusha, V. V. (2011) An enhanced
588   monomeric blue fluorescent protein with the high chemical stability of the chromophore.
589   *PloS one* 6, e28674, doi:10.1371/journal.pone.0028674.

590   Tang, W., Tam, J. H., Seah, C., Chiu, J., Tyrer, A., Cregan, S. P., Meakin, S. O. &
591   Pasternak, S. H. (2015) Arf6 controls beta-amyloid production by regulating
592   macropinocytosis of the Amyloid Precursor Protein to lysosomes. *Molecular brain* 8, 41,
593   doi:10.1186/s13041-015-0129-7.

594   Villegas, C., Muresan, V. & Ladescu Muresan, Z. (2014) Dual-tagged amyloid-beta
595   precursor protein reveals distinct transport pathways of its N- and C-terminal fragments.
596   *Human molecular genetics* 23, 1631-1643, doi:10.1093/hmg/ddt555.

597   Zheng, H. & Koo, E. H. (2011) Biology and pathophysiology of the amyloid precursor
598   protein. *Molecular neurodegeneration* 6, 27, doi:10.1186/1750-1326-6-27.

599

600

Figure 1

Schematic representation of the bioassay rationale.

(a) Design of the various chimeric constructs. The N-terminal tags are inserted after the signal peptide (SP) that target APP to the plasma membrane. HA and AP are two short amino acid sequences. HA is recognized by a specific antibody and AP is biotinylated by a specific enzyme. (b) Once mChAPPmGFP is cleaved by β-secretase, the sAPPβ fragment carrying mCherry (mCherry-sAPPβ) is released into the medium, causing a change in the ratio between the red and green fluorescence intensity.
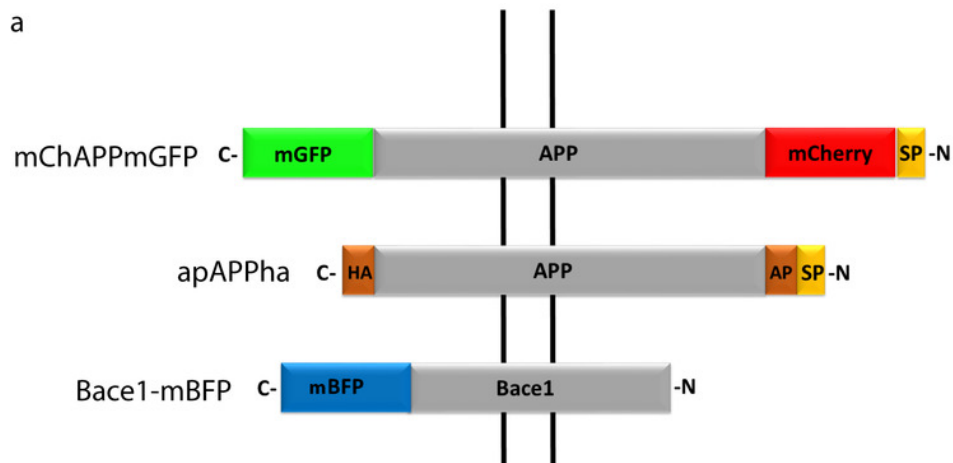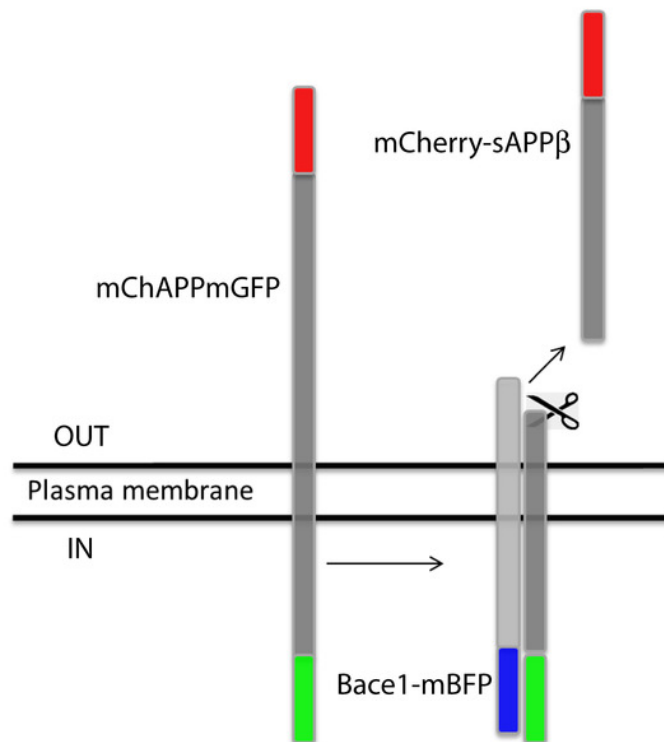
Figure 2

Correct targeting of mChAPPmGFP and colocalization of mCherry and mGFP.

(a) Maximum intensity projection of a confocal z-stack of fixed human SH-SY5Y cells transfected with mChAPPmGFP and surface labeled with anti-mCherry coupled to secondary Alexa 405 antibody (blue). Maximum intensity projections of confocal z-stacks of living human SH-SY5Y cells (b) and rat hippocampal neurons (e) transfected with mChAPPmGFP. (h) Maximum intensity projection of a confocal z-stack of fixed and permeabilized SH-SY5Y cells transfected with apAPPha and labeled with streptavidin Alexa 568 (red), which binds to the bionitylated AP tag, and anti-HA coupled to secondary Alexa 488 antibody (green). The high degree of co-localisation of the red and green signals evident from the linear correlation of scatterplots (c, f, i) and the exponential shape of the Li's intensity correlation analysis (d, g, j) is confirmed by the Pearson's (Pc) and Manders'coefficients (M1 and M2) close to 1, and by the intensity correlation quotients (ICQ) close to 0.5. The probability of obtaining the observed Pcs by chance is inversely correlated with the Costes' randomization P value, which is 100% in all cases. Scalebars, 10 μm.

a
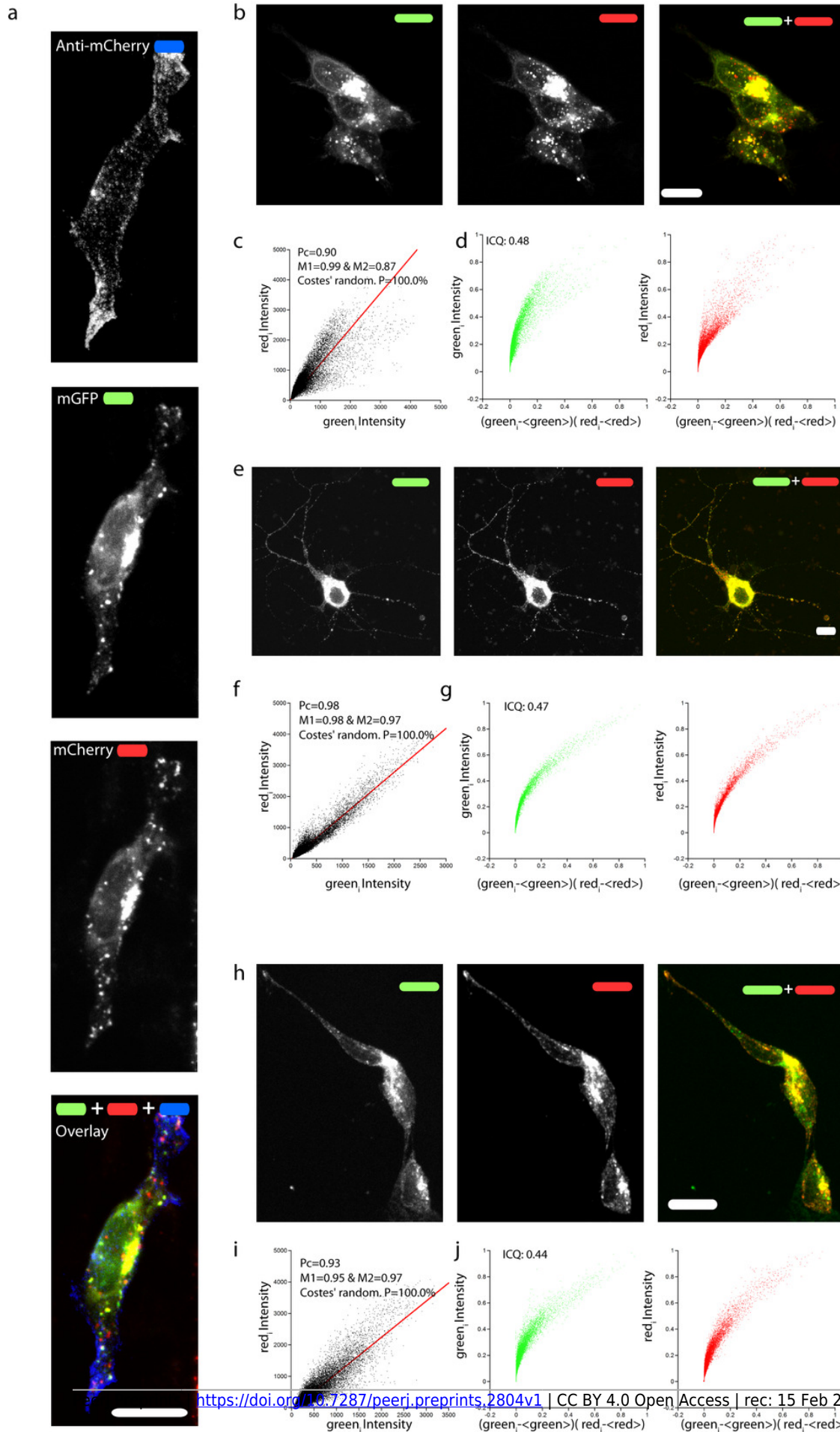
Anti-mCherry

mGFP

mCherry

+ +
Overlay

b

c
Pc=0.90
M1=0.99 & M2=0.87
Costes' random. P=100.0%

green₁ Intensity

d ICQ: 0.48

green₁ Intensity

(green₁-<green>)(red₁-<red>)

red₁ Intensity

(green₁-<green>)(red₁-<red>)

e

f
Pc=0.98
M1=0.98 & M2=0.97
Costes' random. P=100.0%

green₁ Intensity

g ICQ: 0.47

green₁ Intensity

(green₁-<green>)(red₁-<red>)

red₁ Intensity

(green₁-<green>)(red₁-<red>)

h

i
Pc=0.93
M1=0.95 & M2=0.97
Costes' random. P=100.0%

green₁ Intensity

j ICQ: 0.44

green₁ Intensity

(green₁-<green>)(red₁-<red>)

red₁ Intensity

(green₁-<green>)(red₁-<red>)

Figure 3

Red/green fluorescence intensity ratio and intercellular variability of mChAPPmGFP processing.

Maximum intensity projections of confocal z-stacks of living human SH-SY5Y cells (a) and rat hippocampal neurons (b) transfected with mChAPPmGFP. The average red/green fluorescence ratio can fluctuate within the same population of cells (examples indicated by coloured arrows). The red/green ratio image has been mean filtered (2 pixels) only for representation purposes. Scalebar 10 μm.
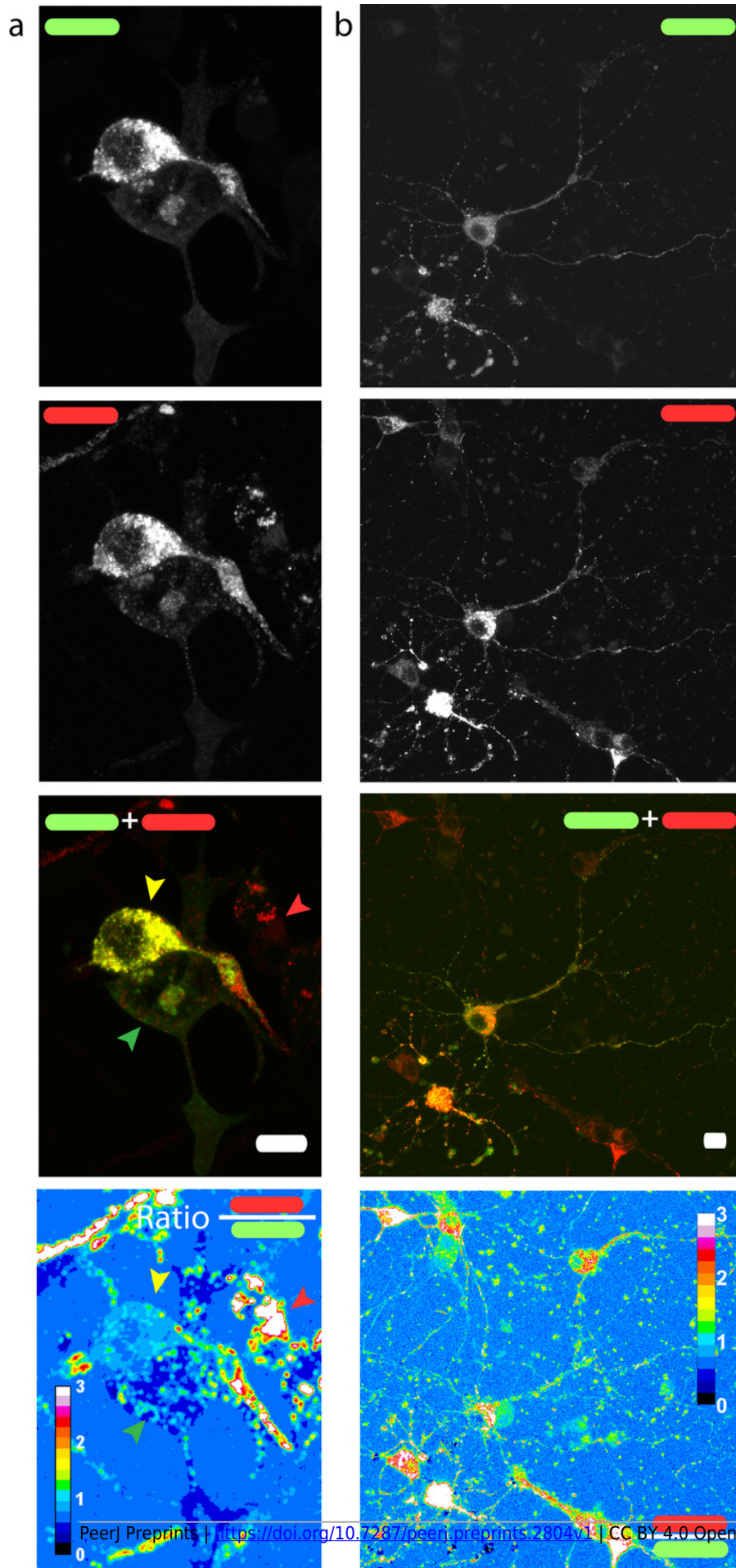
Figure 4

Proof of principle: overexpressed β-secretase cleaves efficiently mChAPPmGFP.

(a) Maximum intensity projection of a confocal z-stack of living human SH-SY5Y cells co-transfected with mChAPPmGFP and Bace1-mBFP. The red/green fluorescence ratio image has been mean filtered (2 pixels) only for representation purposes. Scalebar, 10 μm. (b) The different mean red/green fluorescence intensity ratio values of the two cells outlined in ratio image (a) are correlated to the overexpression of Bace1-mBFP (error bars, s.d.).(c) Dot blot of the mean red/green ratio of SH-SY5Y cells under different conditions of transfection. n > 15 for each condition; ***, p<0.001 according to unpaired Student-t test with unequal variance, run with respect to cells transfected only with mChAPPmGFP or mChAPP770mGFP. (d) Superimposed westernblots of transfected SH-SY5Y cell lysates (magenta) and extracellular media (cyan), labelled with anti-mCherry. The lysate blot was repeatedly stripped and reprobed with anti-GFP, anti-APP and anti-Aβ. The lower band corresponds to mCherry-sAPP, while the higher to full-length mChAPPmGFP. (e) The extracellular medium of SH-SY5Y cells under different conditions of transfection was analysed with a fluorescence spectrophotometer. Emission spectra were collected following excitation at 550 nm.
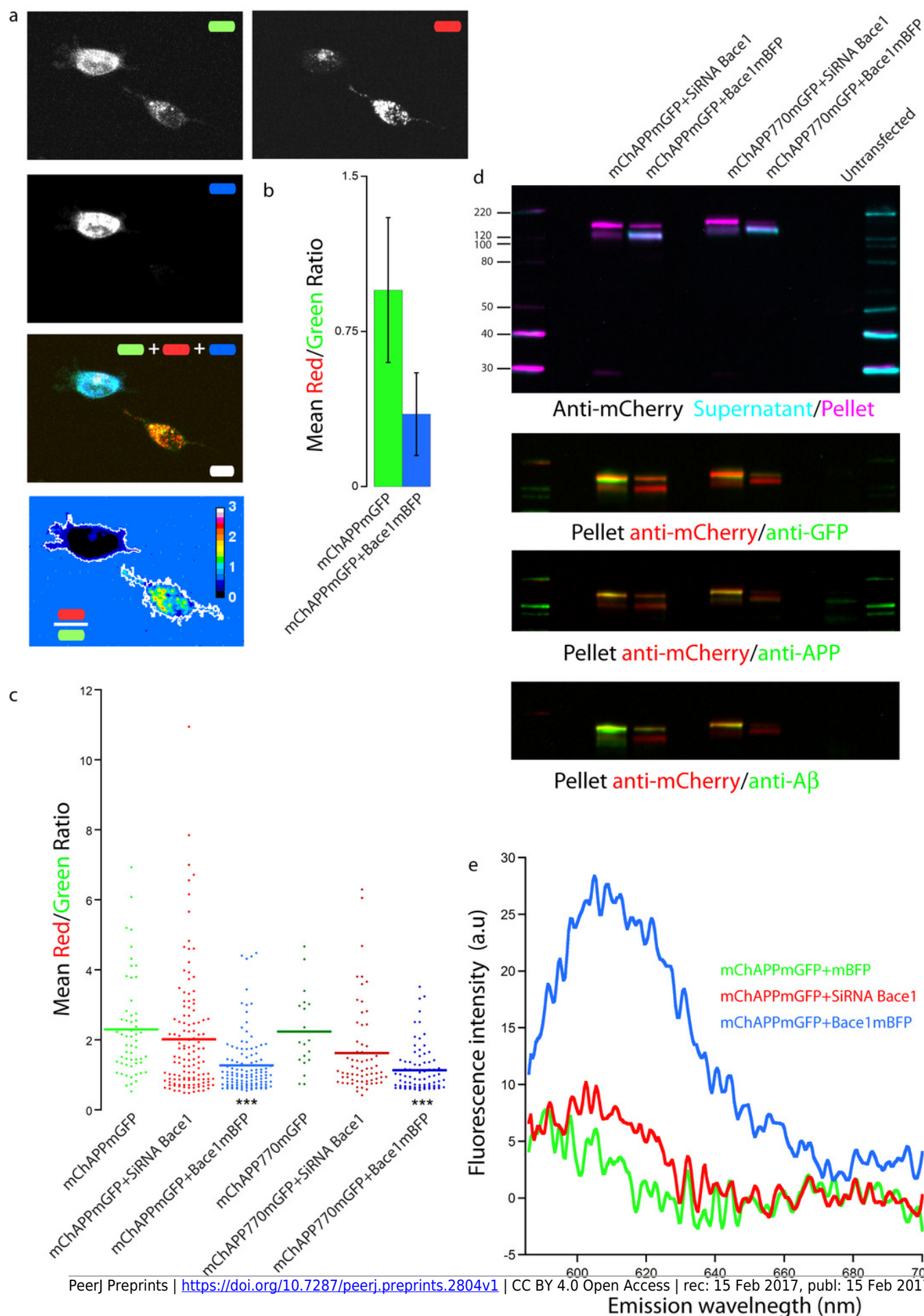
Figure 5

mChAPPmGFP is properly processed in neurons.

Maximum intensity projections of confocal z-stacks of living rat hippocampal neurons co-transfected with mChAPPmGFP and mBFP (a) or Bace1-mBFP (b). The red/green ratio images were mean filtered (2 pixels) only for representation purposes. The insets correspond to the magnified regions outlined in the ratio images. Scalebars 10 μm.
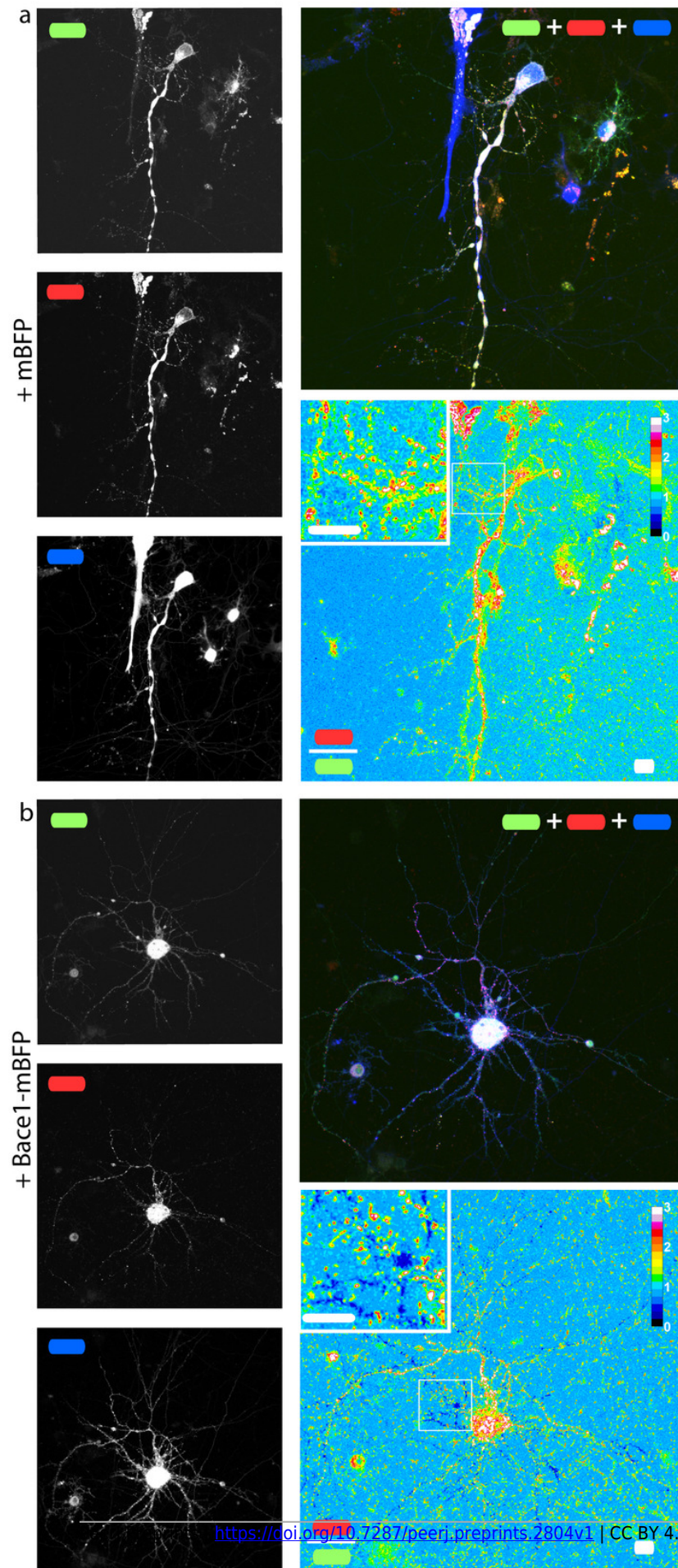
Figure 6

FACS flowcitometry as additional way to screen mChAPPmGFP processing.

(a) Each dot in the scatter plot represents the green and red fluorescence intensity of a single cell. The two different areas (red and green) in the scatter plot were arbitrarily chosen so that both areas contained the same number of SH-SY5Y cells co-transfected with mChaPPmGFP and control siRNA. These regions were used to gate the scatter plots of cells co-transfected with mChAPPmGFP and Bace1-mBFP, Bace1-siRNA, or control siRNA, and calculate the mean ratio between the number of cells in the red area over the number of cells in the green area (b). n = 3 independent experiments; error bars, s.d.; p<0.0001 according to unpaired Student-t test, run with respect to cells transfected with mChAPPmGFP and control siRNA.
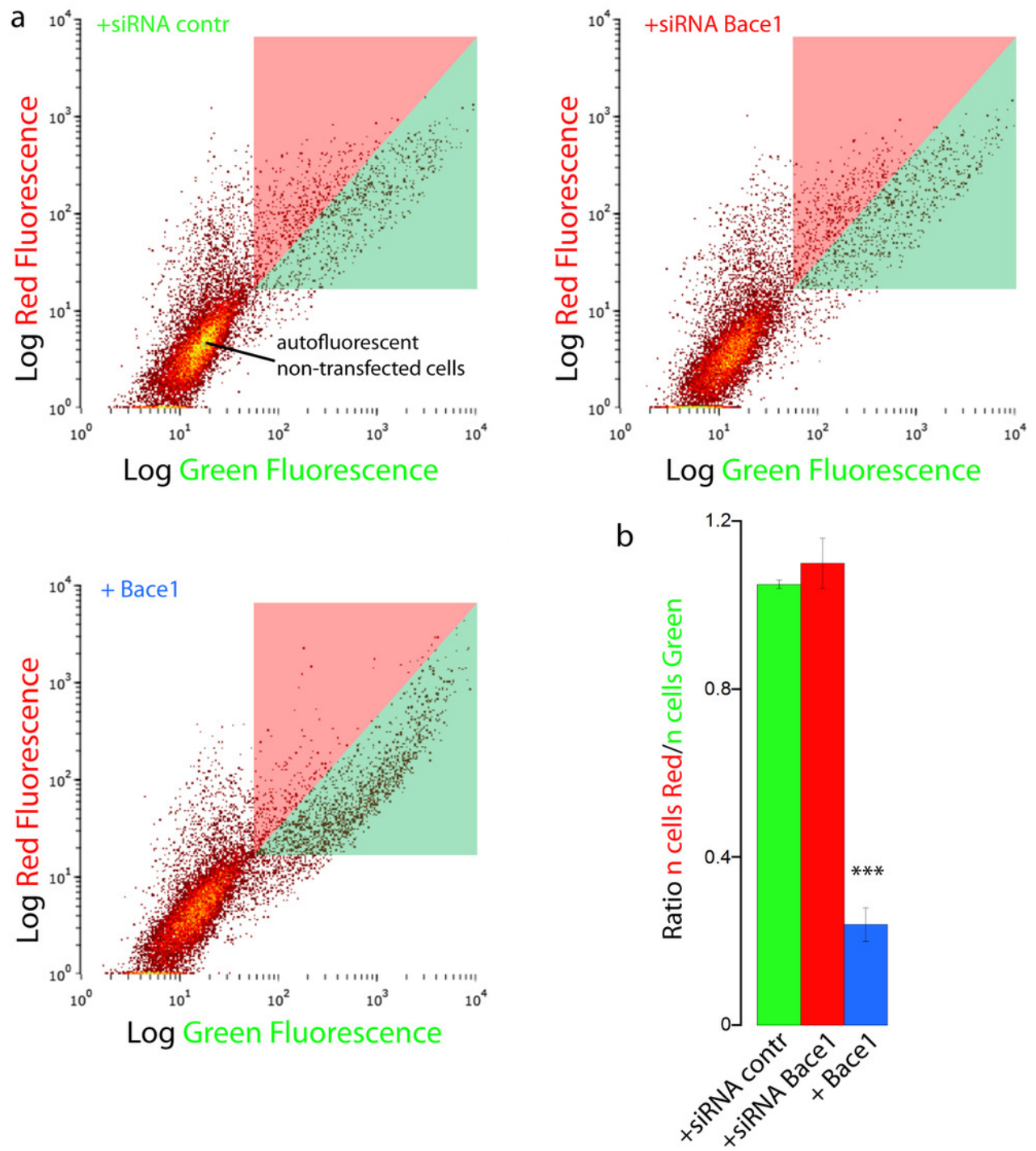
Figure 7

The mChAPP^{P1}mGFP mutant is not efficiently cleaved by the α-secretase ADAM10.

(a) Maximum intensity projection of confocal z-stacks of living human SH-SY5Y cells under different conditions of transfection. The red/green ratio images were mean filtered (2 pixels) only for representation purposes. Scalebar 10 µm. (b) Dot blot of the mean red/green ratio of SH-SY5Y cells under different conditions of transfection. n ≥ 10 for each condition; ***, $p<0.001$ according to unpaired Student-t test with unequal variance. (c) FACS flowcytometry confirms the inhibitory effect of the P1 mutation on α-secretase, but not β-secretase, processing. n = 3 independent experiments; error bars, s.d.; *, $p<0.05$, ***, $p<0.001$, according to unpaired Student-t test with unequal variance. Scatterplots from one experiment are reported in Supplementary Figure S7.